ISSN: 2454-9940

INTERNATIONAL JOURNAL OF APPLIED SCIENCE ENGINEERING AND MANAGEMENT

E-Mail :
editor.ijasem@gmail.com
editor@ijasem.org

www.ijasem.org

INTERNATIONAL JOURNAL OF APPLIED SCIENCE ENGINEERING AND MANAGEMENT

ISSN2454-9940www.ijsem.org
Vol 6, Issuse.4 Oct2018

Grouting duct connectors in precast concrete: an experimental and analytic investigation

Dr.Syed Omer B, Dr.K.Pandu, S Ramya kala

Abstract; Because of their wide tolerances and inability to need welding, grout dowel in conduit connections are often used in the construction of precast walls and bridge bent cap systems. Current design recommendations for this kind of connection regard the duct like any other reinforcing bar in concrete, despite its limiting effect. To learn more about the differences between grouted dowel connections and bar-in-concrete, this study combines experimental and analytical methods. In the experiment, 24 pull-out specimens were evaluated using monotonic stresses. Main factors investigated were embedment length, concrete compressive strength, and duct corrugation. Both theoretical and practical investigations found that grouted dowel in conduit connections behave differently from bars embedded in concrete. A number of grouted connections broke down within the duct because of the tight conditions. In addition, for all embedment lengths, there was an increase in load bearing capacity and ductility of the connections, and this was true regardless of the concrete compressive strength. An analytical model was built to help with the prediction of the outcomes of the experiments.

It was calculated, calibrated, and shown that the link's embedding length was more accurate than standard design techniques.

Keywords ;In this context, the terms "grouted bar," "corrugated duct," "connection," "bond," "pull out," "tensile load," "precast concrete," "model," and "prediction" are all applicable.

1 Introduction and background

The rapidity and precision of plant-manufactured products and the accumulated body of knowledge in the form of design requirements and research data have given precast concrete construction a significant boost over the last couple of decades. Structures made from precast materials may be designed using a variety of strategies. The use of double tees or hollow core floors, both of which can sustain loads, is common with precast load-bearing walls. As a result of its favorable tolerances and the removal of welds, a grouted dowel tie is often used to join vertical precast wall panels on the job site. Tension in a plane due to lateral stresses may also be resisted by this connection. A example wall-to-wall detail with a grouted connection is shown in Figure 1. As a rule, a mechanical coupler is used to span the horizontal junction between two vertical panels and support a reinforcing bar of size No. 8 or bigger. The precast panel incorporates a corrugated metallic conduit, into which the additional length is grouted.

Department of civil
omar.syedomar.syed@gmail.com, pandu.ouce@gmail.com, ramyakala9@gmail.com
ISL Engineering College.
International Airport Road, Bandlaguda, Chandrayangutta Hyderabad - 500005 Telangana, India.

Fig. 1 Schematic diagramshowing a grouted dowel connection

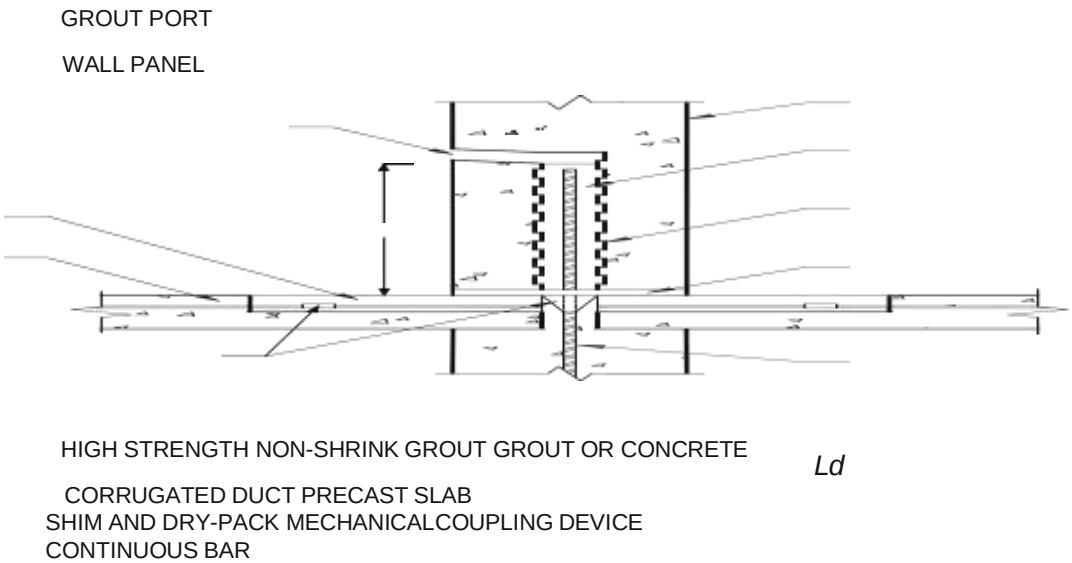

Two ties per panel are required for structural integrity (as per ACI 318-14 Section 16.2.5) [1] and grouted connections must be able to support tensile loads caused by in-plane lateral loads for precast load-bearing walls to be used. The assembly is made more resilient at high levels of seismic stress and damage buildup thanks to the link, which is often a horizontal gap opening between two vertically stacked walls. The bar's giving gives visible evidence of this. The resulting nonlinearity allows for more flexibility and energy release. Due to recent seismic occurrences, it is imperative that these modes be thoroughly investigated. The authors plan to return to this issue in subsequent works.

Grout connections are modeled using the equations defining the evolution of deformed bars under tension, as required by ACI 318-14 and PCI 2010. Table 1 displays a number of formulae used to characterize the development length in tension (where; Ld = develop- ment length in tension; fy = reinforcement yield stress; fc0 = concrete compressive strength; fc0 = Ld).$\frac{c_b}{}$ $\frac{k_{tr}d_b}{}$

d_{duct} = diameter of duct;

b = modification factor for duct material; $f_{s,cr}$ = critical level of stress in rein- forcement; c = modification factor due to group

an impact; fcg0 = grout compressive strength. Although it is generally agreed upon among specialists that bars grouted in metallic ducts have shown behavior significantly different from the bar-in-concrete idealization, no quantitative evidence of this divergence can be found in the publicly available literature.

Among the first investigations on the confinement effect of metallic sleeves was that carried out by Einea et al. [2]. To connect reinforcement bars of varying diameters and embedment depths, they recommended using grout-filled steel tubing as a splice sleeve. By switching up the network topology, we were able to control the level of isolation. All their samples broke because the grout keys sheared and the reinforcing bars pulled out. Deformed bars in grouted sleeves are a typical component of hybrid frames, and Raynor et al. [3] assessed the strength of the connection between them. Short embedment lengths were used in the testing of the bars under monotonic and cyclic loads. The confining effect of the sleeve was shown to be responsible for the increased bond stresses seen in grouted connections. Steuck et al. [4], who tested the strength of large diameter bars grouted in vertical ducts for a bridge bent cap system, obtained similar findings. The

tensile capacity of the embedment could be mobilized at embedment lengths 3 times less than those suggested by ACI 318-05.

According to the aforementioned works, there is broad agreement that the bond failure of deformed bars grouted in corrugated sleeves differs from that of deformed bars in concrete. However, as detailed in Table 1 [4-7], most relevant research is concerned with the use of grouted connections in precast bent cap systems, and often reports empirical models to anticipate the behavior of grouted connections. The findings of these investigations cannot be extended to the behavior of grouted connections utilized in precast walls due to the sensitivity of bond to a variety of relevant circumstances. Given the dearth of data about the performance of grouted connections in precast walls, a tailored experimental technique is introduced here to fill in the blanks. thus the

The purpose of this paper is threefold: (1) to conduct an experimental study of the performance of a typical grouted connection detail; (2) to present quantitative experimental evidence distinguishing the performance of grouted connections from that of bars embedded in concrete; and (3) to develop a credible empirical expression that can estimate the performance of grouted connections and ultimately serve as a user-friendly design tool. The typical bond stress of grouted corrugated duct connections is described in this work based on the results of experimental and analytic- ical programs. In contrast to their duct-less counterparts, grouted connections do not have splitting failures under identical circumstances; this is a result of the corrugated duct's constraining influence.

2 Experimental program

2.1 Test specimens

The experimental program was developed to assess the reaction of specimens under similar circumstances, allowing for a comparison of the behavior of grouted connections and bars buried in concrete. The first set was made up of bars anchored in concrete, while the second set was made up of grouted connections anchored at the same embedment length and put to the same test. Non-reinforced concrete prisms of 203.2 by 203.2 by 406.4 mm were used as examples to represent a typical precast wall, as shown in Fig. 2. Experiments with joint grout

Fig. 2 Test specimens:(*left*) grouted specimen;(*right*) bar in concrete specimen

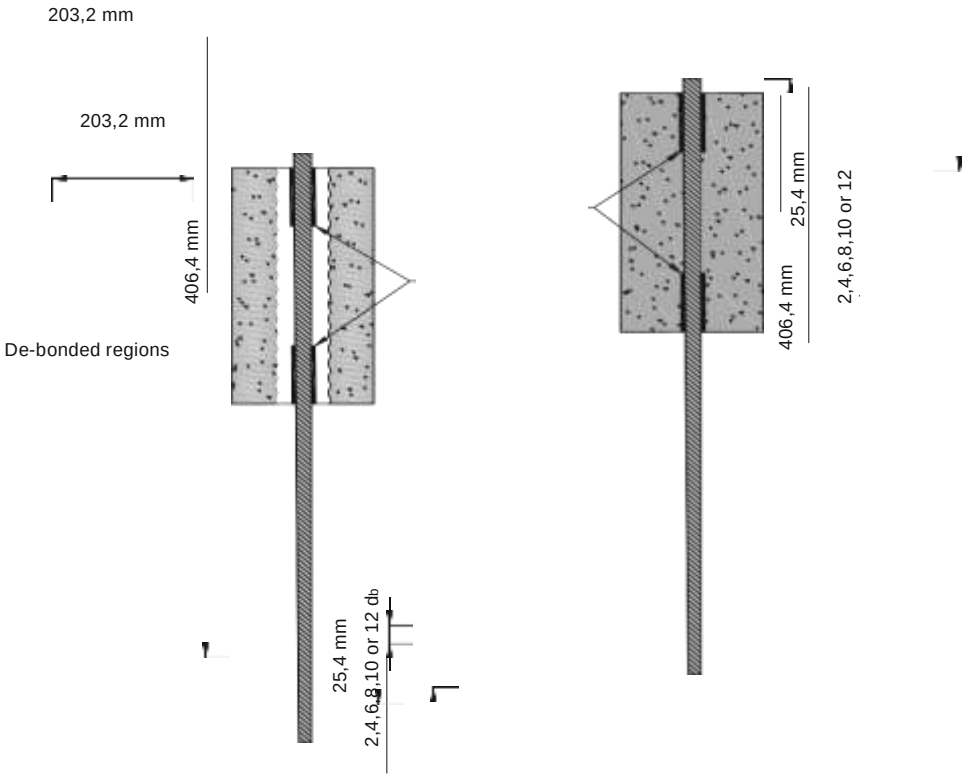

embedding a corrugated steel duct with a 76 mm diameter and 30 guage in a concentric fashion inside the prism. The bars were unbonded by being wrapped in polystyrene wrap 2 mm in thickness. There was a correlation between embedding depth and de-bonded length (2, 4, 6, 8, 10 and 12 db embedment were considered in this study). We selected the embedding lengths such that we could evaluate the bond at both the elastic and inelastic regions of the theoretical stress-slip curve. Non-shrink grout was mixed at low speed for 10 minutes, then at high speed for 5 minutes, adding water until a desirable flowing consistency was achieved, and grouting of the specimens was performed while they were vertical. This followed the concentri- cal placement of the bars inside the corrugated duct.

2.2 Materials properties

Table 2 displays the composition of the concrete mixtures and the mechanical characteristics of the concrete utilized in the investigation. The concrete used in the experiment was factory-made self-consolidating concrete. The ASTM C39 (compressive strength) [8], C496/C496 M (splitting tensile strength) [9], and C469/469 M (modulus of elasticity) [10] methods were used to evaluate the mechanical parameters of the concrete and grout. At 28 days, the average values for the compressive and splitting tensile strengths on three identical 1009200 mm cylinders were 50.6 and 5 MPa, respectively. The joints are sealed using a special, high-strength, non-shrink combination of grout with a compressive strength of 40 MPA and a tensile strength of 6 MPa after 28 days. Each 25 kilogram (55 lb) dry bag was hydrated with 1 US gallon (3.8 l) of water following the manufacturer's instructions for a self-leveling consistency. All samples were cured at room temperature (T = 23 °C) and relative humidity (RH = 60%) for 28 days. Grade 400 No. 8 (25 mm) distorted bars were utilized as connector dowels in the samples. In our investigation, we utilized only steel that came from a single manufacturing run by a single vendor. The mechanical properties of the dowel used as a connection were evaluated in accordance with ASTM 370 [11]. The typical return

Table 2 Concrete mixture design and mechanical properties

Materials	Per 1 m^3	Comp. strength (MPa)							
Age (days)									
Tensile strength (MPa)									
Young's Modulus 910^3 (MPa)									
Poisson'sratio									
		7	28	7	28	7	28	7	28
Concrete									
CSA type 30 cement	435 kg	53.7	61.6	5.1	6.1	26.0	26.0	0.25	0.24
Sand	842 kg								
14 mm aggregate (round)	842 kg								
Water	200 l								
Air	5%								
Air entrainment/lubricant	20 ml/100 kg cement								
High range water reducer	630 ml/100 kg cement								
Grout									
Proprietary high strength non-shrink grout (ASTM C1107)	–	38.4	39.3	4.5	6.3	20.7	22.7	0.22	0.23

stress and the corresponding yield strain were 418 MPa and 0.2–0.6%, respectively. The ultimate tensile stress and strain were 603 MPa and 1.2–1.8%,respectively.

2.3 Pull-out testing

There has been some debate about whether or not pull-out tests are an appropriate way to measure the strength of a concrete and reinforcing joint. The strains at the fixed end of a pull-out specimen are quite different from those experienced in real-world applications. By applying a longitudinal normal compressive field to the concrete, which exposes the bar to tensile stresses, we may artificially improve the bar's bond by confining it more tightly (Fig. 3). This action is further amplified by friction between the specimen and bearing plates. Similar to how confinement, compressive strength, and the bar's physical and mechanical properties are all known to have a significant impact on bond, it is not possible to directly quantify bond using the most standard techniques. The pull-out test, however, is a quick and cheap way to compare anchored bars subjected to the same testing circumstances [4, 6, 8, 9]. Pull-out testing was used in the current investigation, with the aforementioned artifacts mitigated by means of careful thought and planning. First, a 215.9 mm 215.9 mm 25.4 mm hollow steel cradle with a 152.4 mm 152.4 mm aperture was placed underneath the specimen to lessen the confinement close to the bars, and this was done for a length of 5 db in both directions. Second, the tested zone was shifted to locations where the amplitude of the compressive field is lower thanks to the debonding of the bars away from the active end of pulling (where the effects of the induced compression are most evident).

2.4 Test procedure

Two samples were analyzed for each parameter to provide reliable findings. Each specimen was cured at room temperature for 28 days before being put on top of the active pulling end of a 530 kN capacity open loop Tinius Olsen testing machine (see Fig. 4). Prior to commencing testing, the loading machine was calibrated to guarantee that all specimens were subjected to the same load. The load was applied monotonically at a rate of 60 MPa/min, with the bar extended to the bottom plate and grasped by two steel jaws for a length of 165.1 mm. A 25-mm strain based linear variable displacement transducer (LVDT) was used to record the bar's slide.

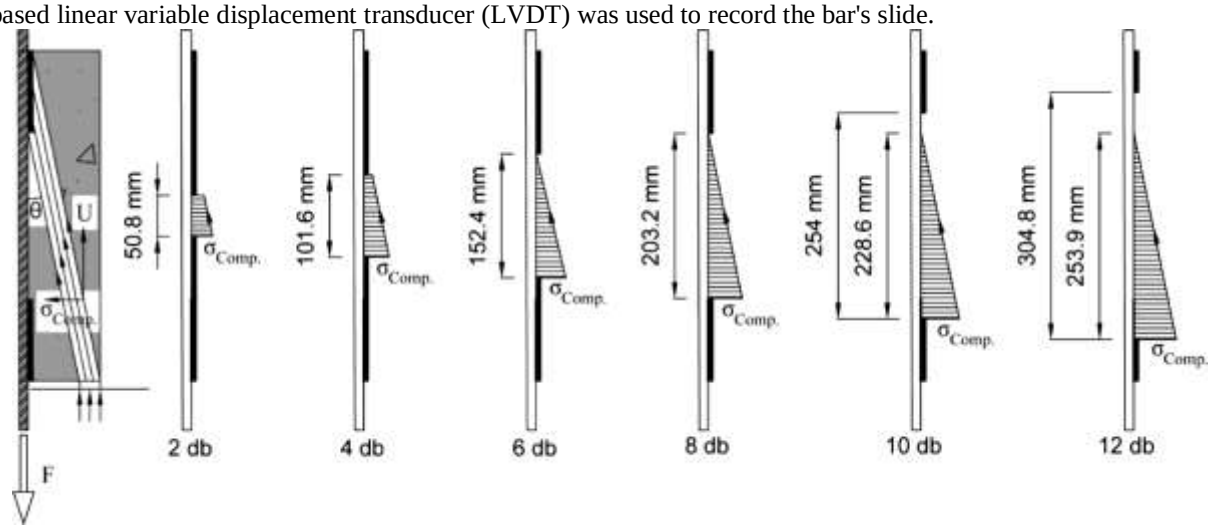

Fig. 3 Strut and tie analysis of the superficial compressive fields resulting from the boundary conditions at: (from *left* to *right*) 2, 4, 6, 8, 10, and 12 d_b embedment length

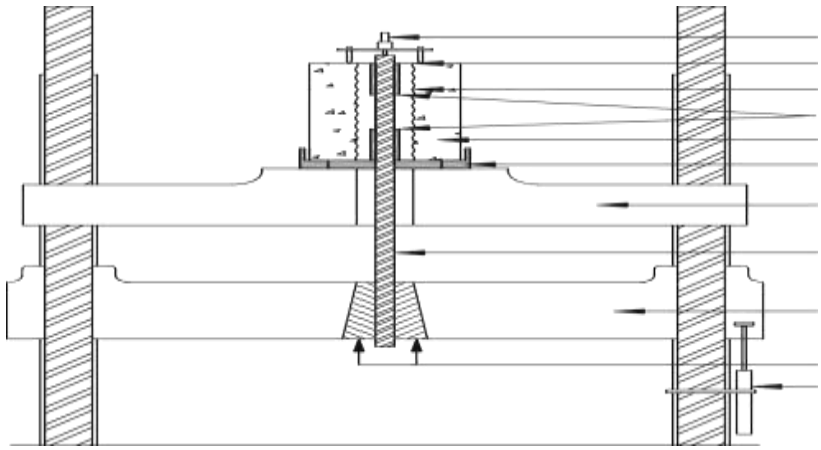

Fig. 4 Test setup and instrumentation

A steel tripod was used to record the slip with respect to the specimen's top surface; it was positioned on the protruding bar from the top (unloaded end). A 150-mm spring LVDT was used to track the elongation of the bar at the loaded end of the specimen by measuring the distance between the machine's fixed and movable heads. Both LVDTs used in the investigation were calibrated using precision gage blocks before each test to guarantee consistent results. A data gathering device took ten measurements per second of the load and slip during the test.

3 Experimental results and discussion

Results from the 24 pull-out test specimens are presented in Table 3 (Where: L_d = embedment length

Table 3 Pull-out test results

Specimen tag[a]	L_d (d_b)	F_{max} (kN)	U_{av} (MPa)	U_{rs} (MPa)	f (MPa)	S_{max} (mm)	D_{max} (mm)	a_{BPE}	K–S	Failure type
Bar in concrete										
C-2-D1	2	60.90	15.02	14.26	120.19	1.33	9.50	0.25	0.49	Pull-out
C-2-D2		74.50	18.38	15.02	147.03	3.22	11.90	0.27	0.45	Pull-out
C-4-D1	4	191.92	23.67	19.18	378.76	1.21	13.50	0.34	0.30	Splitting ? Pull-out
C-4-D2		179.76	22.17	18.78	354.76	3.36	15.40	0.34	0.37	Splitting ? Pull-out
C-6-D1	6	204.80	16.84	5.31	404.18	2.04	17.10	0.32	0.34	Splitting ? Pull-out
C-6-D2		245.52	20.16	NA[b]	484.54	0.78	35.60	0.49	0.32	Splitting
C-8-D1	8	297.33	18.33	–	586.78	0.86	87.00	–	–	Bar fracture
C-8-D2		295.88	18.24	–	583.93	0.62	87.70	–	–	Bar fracture
C-10-D1	10	298.52	14.73	–	589.14	0.06	82.00	–	–	Bar fracture
C-10-D2		296.65	14.64	–	585.45	0.06	81.70	–	–	Bar fracture
C-12-D1	12	297.08	12.21	–	586.29	0.04	74.60	–	–	Bar fracture
C-12-D2		296.33	12.18	–	584.82	0.03	69.81	–	–	Bar fracture
Ducted specimens										
NS-2-D1	2	72.42	17.87	13.57	142.92	0.82	11.60	0.18	0.40	Pull-out
NS-2-D2		76.33	18.12	14.69	150.64	1.07	11.10	0.19	0.35	Pull-out
NS-4-D1	4	214.41	26.45	22.73	423.14	0.60	17.40	0.23	0.39	Pull-out
NS-4-D2		206.35	25.45	21.02	407.23	0.62	12.70	0.26	0.30	Pull-out
NS-6-D1	6	263.97	21.71	19.57	520.95	0.62	33.70	0.23	0.44	Pull-out
NS-6-D2		250.91	20.63	18.86	495.17	0.94	43.51	0.19	0.55	Pull-out
NS-8-D1	8	286.10	17.64	15.65	564.63	0.66	85.10	0.17	0.58	Pull-out
NS-8-D2		287.76	17.75	13.58	567.89	0.66	77.70	0.13	0.56	Pull-out
NS-10-D1	10	285.30	14.08	12.84	563.05	0.56	82.60	0.11	0.53	Pull-out
NS-10-D2		293.38	14.47	13.66	578.98	0.73	93.20	0.07	0.63	Pull-out
NS-12-D1	12	304.90	12.54	–	601.73	0.06	94.60	–	–	Bar fracture
NS-12-D2		303.24	12.46	–	598.40	0.09	98.90	–	–	Bar fracture

F_{max}, ultimate load; f, peak stress in bar; U_{av}, average bond stress, U_{rs}, residual bond stress S_{max}, slip corresponding to maximum bond stress; D_{max}, displacement corresponding to maximum bond stress; K–S, Kolmogorov–Smirnov statistic

[a] NS and C refer to Non-Shrink grout and Concrete, respectively; 2, 4, 6, 8, 10 and 12 refer to the bar embedded length, respectively; D1 and D2 refer to the specimen repetition identifier

[b] Data became unreliable

Fmax = ultimate load; Uav = maximum average bond stress; Urs = maximum residual bond stress; f = reinforcement stress; Smax = slip corresponding to maximum average bond stress; Dmax = displacement at peak load; aBPE = coefficient corresponding to level of confinement) all in decibels. The following names were given to the specimens: The matrix type (NS for non-shrink and C for concrete) is shown first, followed by a numerical value denoting the embedment length (2, 4, 6, 8, 10 or 12 db). The following letters indicate the kind of bar used (D for deformed steel bars), and the following number indicates the specimen's position within its set (1 or 2). Deformed bar connections with embedment lengths of 12 times the bar diameter are designated by the notation NS-12-D2, whereas deformed bars embedded in concrete are designated by the notation C-4-D1.

When the embedment length is more than 3–7 db [12], the assumption of homogeneous bond stress throughout the length of an embedded bar is not an appropriate approximation. Non-linearity in the

distribution is introduced as the length of the embedding becomes larger. The distribution is most concentrated towards the active end of the bar and decreases non-linearly as it moves to the passive end. The precise breakdown of Identifying bond stresses throughout the entire length of a bar requires sophisticated instrumentation. It is for this reason that various studies have found it useful to often use this simplification [2, 4, 13–18]. ACI Committee 408R-03 agrees that "...it is both convenient and practical to consider bond forces as though they were uniform along the anchored, developed, or spliced length of the reinforcement," therefore it's important to note that this assumption has backing from the industry standard group. [19]. Based on this information, we were able to determine the typical bond stress U as

$$U = \frac{F}{\pi d L_d} \quad (1)$$

the force along the embedded length divided by the bar's effective area.*F*

where F is the tensile load; d is the nominal bar diameter; and L_d is the bar embedment length.

3.1 Bond failure mechanisms

Several types of failure were seen during this research, and they are shown in Fig. 5. Figure 6 also displays the failure mechanisms of representative test specimens. The failing bars' profiles may be shown in Fig. 7. Except for those implanted at 8, 10, and 12 db, all concrete specimens failed in a mixed (splitting/pulling-out) manner. All duct specimens (apart from NS-12-D1 and

D2, where a bar fracture occurred. At an embedment

Fig. 5 Failure modes ofdifferent specimens

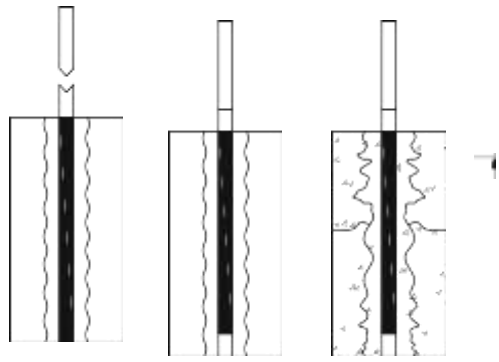

s Bar Pull-out Splitting Bar Fract
(Grouted Specimens) (Grouted/Concrete Specimens) (Concrete Specimens)

Fig. 6 (*Left to right*) Split tensile cracking (C-4-D1); pull-out failures versus splitting failures of comparable specimens at 6 and 4 d_b (NS-6-D1/C-6-D1 and C-4-D2/NS-4-D1, respectively);

and slippage of

(a) (b) (c)

bars versus bar fracture at 10 d_b embedment (C-10-D2 and NS-10-D2)

Fig. 7 (*Left to right*) Wedging of grout keys between ribs in a (C-6-D2); and crushing of grout keys between ribs at 6 and 10 d_b embedment (NS-6-D1 and NS-10-D2, respectively)

Comparable specimens from both groups failed by bar pull-out at a length of 2 db. However, the hoop stress generated by the ribs' contact was insufficient to create a visible splitting failure at this very short embedment length. To a large extent, the bars' slide depends on local failure at the contact between the concrete and the bar ribs. Since the concrete hoop tension was the predominant confining force contributing to the slip resistance, concrete specimens did not split and propagate fractures to the surface when the embedment length was 4 and 6 db (Fig. 6). Longitudinal fractures began forming towards the loaded end of the embedment at 4 and 6 db and spread laterally throughout its length. In Fig. 6, we can see that as the stress persisted, these fissures spread transversely, eventually generating whole separations in the block. As seen in Fig. 7, the bars finally broke apart due to a pull-out with splitting along a plane that ran from the top of one rib to the bottom of the next. The failure mode of grouted specimens with identical embedment (4 and 6 db) was significantly different from that of concrete specimens. Figure 7 depicts the compression failure mode that occurred when the bars in these samples were flexed to their limits. We saw no signs of cracking in the grout cylinder or on the outside of the concrete block (Fig. 8). The ducted sleeve's help in stopping the grout from spreading laterally is shown by the lack of splitting failures at this embedment length. There are three basic reasons in favor of this claim: (3) the additional resistance against slip provided by ducted specimens; (1) grouted specimens consistently achieved higher bond stresses; (2) scatter in results between subgroups of concrete specimens inherent to the nature of concrete exposure to tension (average COV of 70 and 350% for 4 and 6 db, respectively); and (1) the additional resistance against slip provided by ducted specimens (Fig. 10). The average recorded tensile capacity was achieved in tests on concrete specimens with bars implanted at 8 and 10 db, with the specimens failing due to bar rupture at this stress. Comparable grouted specimens failed, as seen in Fig. 7c, due to pull-out of the bars caused by shearing of the grout keys, much like their 4 and 6 db counterparts. It is important to note that the grout keys were crushed during the failure of grouted specimens no matter what the bond tension was.

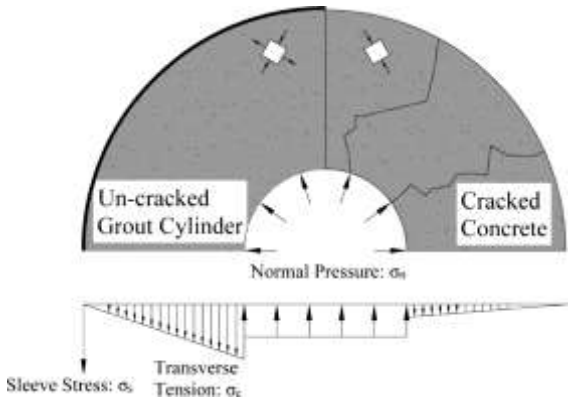

Fig. 8 Stress state inside a corrugated sleeve grouted connec- tion versus cracked concrete cylinder

This observation, when viewed considering the bar strain levels (Fig. 11), reveals that the bond of grouted connections did not seem to be affected by the level of strain of the bar, but rather by the amount of slip mobilized unto it.

3.2 Bond stress–slip behaviour

Figure 9 depicts a comparison between the bond behavior of grouted and sleeve-less concrete sample (represen- tative specimens at different embedment lengths). It was determined what constitutes a "normal" stress-slip reaction in bonds:

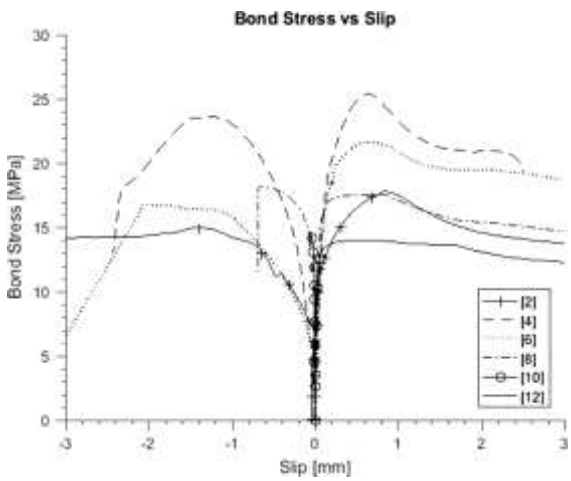

Fig. 9 Bond stress versus slip response of representative grouted specimens (positive slip) and concrete specimens (negative slip) at 2, 4, 6, 8, 10 and 12 d_b embedment

a steepening branch follows a steepening one, and there is an ascending branch where the greatest bond plateaus over a particular slip domain. Predominant slip was seen in the softening branch of the bond-slip response of grouted specimens (Fig. 9). Although this tendency was consistent throughout all embedding lengths, there were clear disparities in the reactions of the two kinds of specimens.

The ascending branch of the bond of grouted connections seemed to have a stiffer reaction up to an embedment length of 8 db. When similar specimens failed in a pull-through mode rather than a bar fracture, the greater stiffness of grouted specimens was brought to light. As expected, this was most prominent at 4 and 6 db embedment lengths, where the loading situation imposes crucial hoop tension values. In addition, at embedment lengths of 2, 4, and 6 db, the average bond stress of the grouted specimens was 7.7, 13.2, and 14.4% higher than that of the concrete specimens.

It's crucial to look at the slip domain across which the nominal rise in maximum average bond stress occurred. As an example, the slip measured for each specimen was normalized by the slip measured at the highest bond tension (Table 3: Smax). In Figure 10, the slip is shown against its value after being normalized by the slip at maximum bond tension. The slope of the line depicts the amount of slip under the given bond stress, with a steeper slope suggesting more slip. Regardless of embedment length, Fig. 10 shows that grouted specimens had less slide than their concrete counterparts. While bar slippage in concrete was rather low at longer development lengths, it increased noticeably at shorter times. The concrete cover's dilatation after being subjected to high tensile loads was blamed in part for this. Furthermore, the grouted connections possessed a stopping mechanism thanks to the corrugated duct's confinement effect. Variations in specimen failure from mixed/pull-out to bar

fracture resulted in slopes that were comparable to one another (10 and 12 db).

After reaching maximum bond tension, comparable concrete sample had a steep softening branch. The remaining bond stress after maximum stress has been reached may be used to dig further into this.

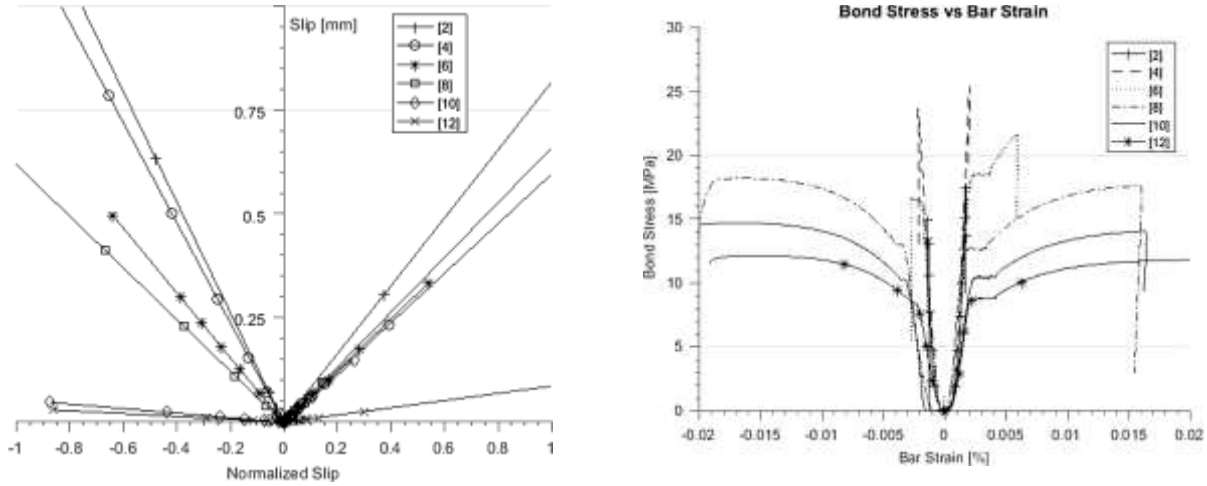

Fig. 10 Comparison between slippage of bars at different embedment: (*left*) concrete; (*right*) grouted connections

which describes the bond behaviour after reaching its maximum capacity, giving insight into the additional resistance along the failing branch of the bond stress– slip response. Residual bond stresses were extracted by examination of individual bond–slip curves of grouted and concrete specimens via determining the corresponding bond stress of the point on the softening branch at which either a flattening of the curve or a sudden change in slope occurred. The recorded valuesare given in Table 3. Grouted specimens achieved an average residual stress increase of 4.9, 15.9 and 72% at 2, 4 and 6 d_b, respectively. A possible reason would bethe normal confining pressure of the corrugated duct specimens, enhancing the frictional aspects of the bond, which was not engaged until the rib bearing components of bond have been exhausted.

3.3 Bond stress–bar strain behaviour

An LVDT was attached to the testing machine and used to track the distance the moving and stationary heads traveled to determine the length of the bars (Fig. 4). All experiments began with the same conditions, with no variation in the distance between the stationary and mobile heads. As a result, we measured from the top of the grips to the bottom of the unbonded section to get an estimate of the bars' original length. The unloaded end slip was recorded and subtracted from the measured elongation to adjust for any errors. The average strain was determined by knowing the starting and ending lengths of the bars under test.

Bond stress versus bar strain for typical samples is shown in Fig. 11. Embedded bars (left) and grouted connections (2, 4, 6, 8, 10, and 12 db embedment) (right) in concrete.

Bond behavior (and its related failure) under different bar strain levels may be understood with the help of Figure 11, which illustrates the average bond stress against strains (elastic, yielding, and plastic). By comparing concrete and grouted specimens with a 2 db embedment length, we find that the bond stress and strain values are similar (0.1%). That fits well with the failure trends we discussed before. With the same strain (0.20 and 0.21% for grouted and concrete, respectively), the grouted specimens showed a 7% improvement in bond at 4 db. Upon visual inspection, there was no evidence of bar yielding. Nonetheless, this amount of strain is quite similar to the yield strain obtained from test coupons (0.2-0.6%). However, unlike similar concrete specimens, tensile failure was not

triggered by the increase in bond stress in the grouted specimens. The average compressive strength of the concrete samples after 28 days was 56% greater than that of the grout. A yield plateau was clearly apparent at 18.53 MPa for the grouted and 16.51 MPa for the concrete specimens at 6 db embedment, with splitting fractures dominating the pull-out failure of the concrete specimens. The grout keys in the failing specimens were crushed (pulled out) at the strain hardening zone. It's worth noting that even though the highest average bond stress was 18.24 MPa (a 10.5% increase from 6 db embedment), the concrete block did not develop splitting fractures at 8 db. This is due to the incorporation of extra bar ribs, which decreased the tension in the transverse direction on the concrete cover due to the increased surface area of the ribs. Results from 8 and 10 db of embedding grouted samples inA_s ¼

3.4 Analytical analysis

Consideration was given to the analytical bond-slip law presented by Eligehausen et al. [20] (BPE model) in an effort to simulate the behavior of grouted connections. Several research, such as [7, 9–11, 21], have used this model to explain the analytical behavior of bars buried in concrete, and it has been accepted by the CEB- FIP code 1990 (MC90). Pull-out was used to generate average bond stress using Eq. (1) and free-end slip values were measured and presented in Table 3 to calibrate the model. Following is a

$$\frac{s}{s_{max}} = \left(\frac{s}{s_{max}}\right)^{a} \quad \text{ð2Þ}$$

greatest relative dissimilarity between the two distributions, expressed as a numeric value between 0 and 1 [24]. As a result, the K-S statistic is an effective instrument for

Bond stress and slip at each loading increment are denoted by s and s, respectively; maximal average bond stress and slip are denoted by smax and smax, respectively; and an is a model fitting parameter.

MC90 states that for a value of a to have physical significance, it must fall between 0 and 1, with a value of 0.4 being the sweet spot for both confined and unconfined concrete [22]. A smaller value for a

mathematical expression for the BPE model's ascending branch (s B s1):
where The region underneath the growing shoot is, too.

with respect to each specimen.
Areas beneath the ascending branch of the experimental data were used to determine the value of a, which was then used to calibrate the parameter (3). While the two regions were equalized, attention was made to maintain the curve's overall shape [23]. The initial focus was on calibrating the model for grouted connections, but this was broadened to include the concrete cohort to allow for a direct comparison of the two. Table 3 displays the obtained values of for each specimen (failed in pull-out).
Two-sample Kolmogorov-Smirnov testing was used to examine the goodness-of-fit, allowing for a more direct comparison between the experimental and theoretical outcomes (K–S test). Since the K-S test compares the experimental and analytical data at each point, it can detect changes in distributions wherever they occur and to whatever degree they occur. The Kolmogorov-Smirnov statistic (K-S stat) is a scalar test statistic that is often calculated by taking the difference in cumulative frequencies of two distributions. indicates a more flexible reaction, with a sharp rise in bond stress occurring without significant slip for values closer to 0. When the slip domain lies between s1 and s2, the model predicts an area of constant bond stress (s = smax), and the behaviour of the softening branch of the bond (s2 s s3) is described by a linearly falling branch. When s = sf is applied to s [s3, the friction is represented by a horizontal branch. Therefore, a, s2, s3, and sf must be calibrated using experimental findings in order to update the model to reflect the present condition.

Cosenza et al. [23] provided the following connection for determining an appropriate value for the parameter a:

analyze congruence in light of Table 3 data. The K-S values that have been published suggest that the experimental and analytical findings are consistent.

Each specimen's calibrated parameter a was utilized

to draw its respective analytical envelope. Figure 12 depicts, for typical specimens with 4, 6, 8, and 10 db embedment lengths, comparisons between the experimental and projected analytical curves of grouted connections. The analytical and experimental curves show a strong correlation. One key finding is that the lengthier embedment yields more accurate analytical predictions of the horizontal branch at maximum bond stress (8 and 10 db).

The parameter a ranged from 0.25-0.49, with a mean value of 0.34, according to the analytical findings of the concrete samples. The range for comparable grouted specimens was 0.18 to 0.26, with a mean value of 0.18. There was less of an increase in the observed values for parameter a, suggesting a

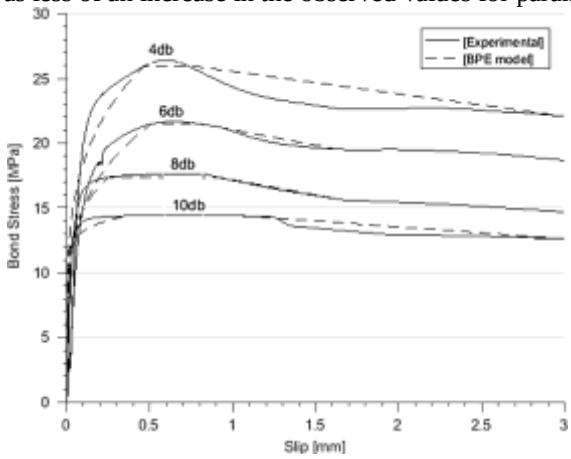

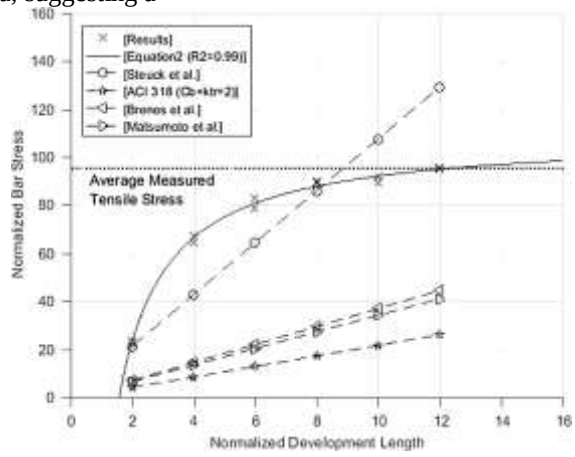

Fig. 12 Experimental results versus analytical predictions ofgrouted specimens based on the BPE model

Fig. 13 Predicted bar stress at corresponding developmentlength of various models (Table 1)

vertical stem rigidity in stone and cement specimens. Despite grout's reduced compressive strength, grouted samples showed a steeper ascending branch. It is thought that the pressure within the duct acted to constrain the grout, so increasing the bond strength.

4 Discussion and implementation fundamentally relies on ignoring the nonlinear changes of the bond stress, which tends to rise with the increase in embedment and assuming uniform stress distribution throughout the length of produced bars.

Using a power regression curve with 98% confidence, the pull-out findings from the five Research looking at grout connections for bridge bending applications are principally responsible for proposing this [4-6]. Such equations are empirical expressions (Table 1) that use a similar approach to the ACI 318-14 that was produced by Orangun et al. [25] by using statistical methods. It's important to note that current design practices provide a maximum confinement factor cbktr of 2.5 for confined concrete, whereas a value of 1 is advised for more cautious outcomes. In Fig. 13, we can see how the different models' predictions compare to one another. The created models show a linear connection between the development length and the normalized bond stress,

embedment lengths (ten specimens) investigated in this research were presented, allowing for easier comparisons with earlier formulae. Here is the form of the resultant equation:

Currently, grouted connection design follows the ACI c 318-14 standard, which was established after the discovery of tensioned reinforcing bars. Numerous design equations have

$$_{s}L_{d} \text{ ¼ } d_{b} \quad 0{:}629 - 0{:}0057 \frac{s}{g} \text{Þ} f \text{ ð4Þ}$$

and therefore with the stresses produced in the bar, which is a major flaw. These representations do provide user-friendly, simplified design statements, however they are not intended for

where Ld is the anticipated development length, fg0 is the grout compressive strength, cs is a steel stress normalization factor, and fs is the stress in the steel connection.

Eq. (4) (2, 4, 6, 8, and 10 db) was derived using only pull-through failures in grouted specimens. It is noteworthy to notice that the predicted normalized bar stress at 12 db is 0.31% less than the average

reported from the experimental data, given that the suggested equation was designed to characterize development lengths that mobil- ize the tensile capacity of bars. A bar's growth time may be determined at any stress level. Figure 13 shows how the predictions of the different models (Table 1) relate to Eq (4). The ACI 318-14 equation's forecast of the stress level is proven to be very cautious for a given development length. It's this

resulting from the intrinsic dissimilarity between grouted connections and the predicted behavior of bars in concrete in the ACI 318-14 model. Even though a greater duct-to-bar diameter ratio was chosen, the development length requirements were still overestimated by the Stueck et al. [4] model. However, Brenes et al[5] .'s and Matsumoto et al[6] .'s predictions understated the degree of stress because of expected failures that were not seen here. The expression for cs is:

$$c_s \quad 605 \quad \frac{f_t}{\delta}$$

5Þ

, where ft is the connector's tensile strength. Variations in steel's tensile strength are accounted for and Ld is adjusted by the factor cs. To fracture a bar made of steel with an average tensile strength of 680 MPa, as opposed to the 12 db required for the steel utilized in the current investigation, an embedment length of 13.6 db would be required.

Paragraphs 5 Concluding Remarks

To investigate how bars behave differently when grouted in corrugated ducts as opposed to concrete, an experimental program was designed. The experimental data were subjected to a regression analysis, which allowed for the derivation of an empirical expression that accounts for the elements impacting the bond. The findings were then compared to the existing ACI 318-14 equation and other pertinent data found in the public literature. Moreover, the experimental bond stress vs slip envelopes were used to calibrate the well-known BPE model. From the results of the foregoing analysis and experimentation, we may deduce the following:

The bond of grouted connections did not break in splitting under identical circumstances and at any stress level in the bar. A preferred pull-through mechanism, compression failure shown as crushing of grout keys between succeeding ribs. Split tensile fractures and bar pullout occurred in control bar-in-concrete specimens.

For a given embedment length, the maximum average bond stress in grouted connections was always higher than in concrete. After the average bond stress had reached its maximum value, the slip readings were similarly lower, suggesting a more rigid ascending branch. After reaching maximum values, the softening branch of the bond stress-slip curve for grouted specimens showed greater ductility with improved frictional resistance compared to bars in concrete.

It was shown that the embedment length had a significant impact on the load bearing capacity of specimens, but could not be used to identify the failure process. Dowel bar strain was greatest at shorter embedment lengths and was equivalent at 8 db of development length. At 12 db of embedment, the bar reached its maximum capacity. When subjected to 6 db of pressure, the bars eventually gave way, but the bond eventually broke at the strain hardening region. When comparing grouted and concrete connections with the same embedment length, the bar strain had no discernible influence on the former but was harmful to the latter's failure.

The calibrated BPE model's predictions were in good enough agreement with the experiments to be considered reliable. Parameter a values for grouted connections were consistently higher than those for their bar-in-concrete analogues, indicating a stronger reaction.

5. Regression analysis of the experimental findings was used to create a design equation. The equation provided a satisfactory prediction of the behavior at 12 db. The compressive strength of the grout, the tensile strength of the bar, and the variability in the ultimate strength of the bars are all included into this equation.

5 Further research

With this research, we want to learn more about how grouted duct connections in precast wall applications respond to monotonic tensile stresses. There has to be further research on the cyclic behavior and eventual bond breakdown. The findings of these experiments should either verify the correctness of Eq. (4) or suggest adjustments to the equation to better account for seismic impacts. The research was done on the premise that the bonding of grouted connections is dependent on the same factors as bars in concrete. The fact that the

The corrugated duct served as a containment effect, and the failure causes were quite different from those of the bar-in-concrete model. The writers have conducted an intensive research project to learn more about this. The results of this research should pave

the way for the creation of analytical and numerical tools that can be used to undertake a parametric examination of the known elements that affect bond.

References

1. The ACI 318 Committee (2014) Code Requirements for Structural Concrete in Buildings, ACI 318-14, with Commentary

2, Einea A, Yamane T, Tadros MK (1995) Joints between pipes in prefabricated concrete are filled with grout. PCI J 40(1): 82–93

Authors: Raynor DJ, Dawn EL, Stanton JF (2002) Grout's effect on bond-slip behavior of reinforcing bars in ducts. 568-576 is the page range that the 99th issue of the ACI Structural Journal covers.

Steuck KP, MO Eberhard, and JF Stanton (2009) Anchorage of large-diameter reinforcing bars in ducts. The article's citation is: ACI Struct J. 106(106):506-513.

Anchorage requirements for grouted vertical-duct connections in precast bent cap systems.pdf 5. Brenes FJ, Wood SL, Kreger ME (2006)

Development of a precast concrete system. Matsumoto EE, Mark C, Kreger ME, Vogel J, and Wolf L. (2008). PCI J 53(3):74–86

7 A. Einea, S. Yehia, and M. K. Tadros (1999) Concrete joints that are lapped. In: ACI Struct J. 96(6):947-955.

Standard Test Method for Compressive Strength of Cylindrical Concrete Specimens, ASTM International, 2016. The American Sociological Association Test Materials 04.02:1-7

ASTMC496/C496M-11 Standard Test Method for Splitting Tensile Strength of Cylindrical Concrete Specifications, American Society for Testing and Materials, 2011. Am Soc Test Matrix 04.02:1-5

Standard test technique for static modulus of elasticity and Poisson's ratio of concrete under compression: ASTM C469/C469M-14 (2014, American Society for Testing and Materials). A sample of the American Sociological Association's Test Materials 04.02:1-7

Standard Test Methods and Definitions for Mechanical Testing of Steel Products, 11th Edition, ASTM International, 2014. 01.03:1-50 American Sociological Association Test Materials

Reinforcement and concrete bond state determination throughout the development length. Tastani SP, Pantazopoulou SJ, 2013. J. Struct. Eng., Part A, 139(9):1567-1581

13 : El Refai A, Ammar M, Masmoudi R (2015) Performance of polymer bars reinforced with basalt fiber under compression. Articles 1-12 (Vol. 19 No. 3 of the ASCE Journal of Construction Materials and Technology)

Bond stress slip response of bars inserted in hybrid fibre reinforced high performance concrete. Ganesan N, Indira PV, Sabeena MV. 2014. The Construction and Building Materials 50:108-115

Post-yield bond behavior of bent bars in high-strength self-compacting concrete. Ashtiani MS, Dhakal RP, Scott AN. 2013. Journal of Constructional Materials 44:236–248

Direct stress pullout bond test: experimental findings. Tastani SP, Pantazopoulou SJ, 2010. 731-743 J. Struct. Eng.

El-Hacha, R., El-Agroudy, H., and Rizkalla, S.H. (2006) How high-strength steel is bonded into place. For the full citation, please use: ACI Struct J. 103(6):771-782

The list of authors includes 18 names: Marchand P, Baby F, Khadour A, Battesti T, Rivillon P, Quiertant M, Nguyen H-H, Ge'ne'reux G, Deveaud J-P, Simon A, and Toutlemonde F. (2015) Connectivity of reinforcing bars in ultra-high-performance concrete. Materials and Structures 49(5):1979-1995

On behalf of the ACI 408 Committee (2003) ACI 408-03, pages 1-49, discusses the bonding and development of tensioned straight reinforcing bars.

R. Eligehausen; E. Popov; V. V. Bertero (1982) Bar deformations and the stress-slip connections between local bonds are studied for a variety of excitations. Published in the proceedings of the 7th European Conference on Earthquake Engineering, pages 69–80

Acklides, Z., Pilakoutas, K., 21st (2004) The pullout behavior of bonded polymer bars with fiber reinforcement. 22: Comite Euro-International Du Beton (1993) CEB-FIP Model Code 1990 J. Compos.

Authors: Cosenza E., Manfredi G., and Realfonzo R. (1997) How FRP rebars behave and how they connect to concrete is modeled. The first issue of the Journal of Composites and Composite Structures was published in 2005, with a focus on the construction

The Kolmogorov-Smirnov test for determining statistical significance. In the Journal of the American Statistical Association 46(253), pages 68-78

A reevaluation of test results on developmental length and splices; Orangun CO, Jirsa JO, Breen JE (1977). Journal of the American Constructive Association, 1974, vol.74, no.3, pages 114–122.